# Impingement Flow Study on Temperature Profile of Concave Plate


By:

**WONG KOK YUNG**

(Matric No: 137869)

Supervisor:

**Dr. Mohd Azmi Bin Ismail**


This dissertation is submitted to

Universiti Sains Malaysia

As partial fulfilment of the requirements to graduate with honors in

**BACHELOR OF ENGINEERING (MECHANICAL ENGINEERING)**


School of Mechanical Engineering

Engineering Campus

Universiti Sains Malaysia


**12th July 2021**

## DECLARATION

This work has not previously been accepted in substance for any degree and is not being concurrently submitted in candidature for any degree. I hereby declare that this project entitled “Impingement Flow Study on Temperature Profile of Concave Plate” submitted to Universiti Sains Malaysia is based on my original work except for quotations and citations which have been duly noted by explicit references.

WONG KOK YUNG
Date: 12/7/2021

# ACKNOWLEDGEMENT

It has been a tough and meaningful journey to complete the thesis in the midst of COVID-19 pandemic. The completion would not be easy without the help of many people. I would like to thank all parties who helped me along the journey including my supervisor, librarians, friends and parents.

Firstly, I would like to express gratitude to my supervisor, Dr. Mohd Azmi Bin Ismail, who has been helpful and patient with me throughout my research progress. He taught me on Ansys Fluent which is a useful software for the thesis. He constantly helped me when I faced problems by giving advice. He is great in giving valuable feedbacks on my work.

I would also thank to the librarians at Universiti Sains Malaysia Engineering Campus who have been helpful in assisting me by providing workshops. I learnt on the techniques to search journals and thesis formatting which are very important for the thesis.

I would also thank to my friends for responding to my questions and giving me advice on the use of Ansys Fluent. They are responsive in answering my questions regarding the software.

Lastly, my sincere thanks to my parents who are supporting me throughout my time in home. Their encouragement provides me energy to move forward.

TABLE OF CONTENTS

# LIST OF TABLES

**Page**

## LIST OF FIGURES

**Page**

## LIST OF SYMBOLS

| | |
|---|---|
| $Nu_0$ | Nusselt number on impingement point |
| $Re$ | Reynolds number |
| $H$ | Distance between nozzle and plate (mm) |
| $D$ | Diameter of nozzle (mm) |
| $R$ | Curvature radius of concave plate (mm) |
| $r$ | Radial distance from impingement point (mm) |
| $v$ | Velocity of air (m/s) |
| $\mu$ | Dynamics viscosity of air (kg/m·s) |
| $A$ | Area of concave plate ($cm^2$) |
| $\rho_{air}$ | Density of air ($kg/m^3$) |
| $h$ | Local heat transfer coefficient ($W/m^2 \cdot K$) |
| $q$ | Dynamic Pressure (Pa) |
| $\emptyset_q$ | Heat flux ($W/m^2$) |
| $\lambda_{air}$ | Thermal conductivity of air (W//$m \cdot K$) |
| $T_0$ | Temperature of impingement point (°C) |
| $T_{point}$ | Temperature of certain point (°C) |
| $T_{ambient}$ | Temperature of ambient air (°C) |
| $T_{air}$ | Temperature of air (°C) |
| $T_{avg}$ | Average temperature of concave plate (°C) |
| $Q$ | Heat transfer rate ($W$) |
| $h_{convection}$ | Convection heat transfer coefficient ($W/m^2 \cdot K$) |
| $\Delta T$ | Temperature difference (°C) |

## LIST OF APPENDICES

# ABSTRAK

Sistem anti icing dipasang untuk mencegah pembekuan ais pada badan pesawat. Sistem ini amat penting untuk memastikan keselamatan pesawat kerana pembekuan ais mengurangkan prestasi pesawat dan boleh menyebabkan kemalangan. Aliran hentaman udara panas dari tiub Piccolo menyebabkan titik panas pada badan pesawat. Pemanasan boleh menyebabkan tekanan terma dan merosakkan badan pesawat. Oleh itu, profil suhu selepas mengalami aliran hentaman udara panas harus diselidik untuk memperbaiki rekaan system anti icing ini. Hentaman udara panas ini disimulasikan dengan menggunakan ANSYS Fluent 19.2. Plot kontur suhu untuk piring cekung telah diperoleh dari perisian. Pengesahan telah dibuat dengan menggunakan korelasi nombor Nusselt pada titik hentaman udara dan nombor Reynolds. Suhu tanpa dimensi meningkat apabila nombor Reynolds meningkat dan suhu udara mengurang. Suhu dimensi tertinggi ialah 0.147125 yang berlaku apabila jejari 300mm, suhu udara 43°C dan nombor Reynolds 4070. Suhu tanpa dimensi berkurang apabila jejari piring cekung berkurang. Hal ini disebabkan oleh penambahan kehilangan panas kepada sekitarnya. Suhu tanpa dimensi bertambah dari 0.138747 kepada 0.142316 apabila jejari piring cekung bertambah dari 150mm kepada 300mm.

**ABSTRACT**

Anti-icing system is installed to prevent ice accretion on the body of aircraft. The system is important for aviation safety because ice accretion degrades the performance of the aircraft and may cause air crash. The impingement flow of hot air from Piccolo tube creates hotspot on nacelle lip skin and edges of wings. Improper heating may cause high thermal stress and damage the nacelle lip skin and edges of wings. Therefore, temperature distribution caused by the impingement of hot air must be studied for better design of anti-icing system. The impingement of hot air was simulated by using ANSYS Fluent 19.2. The temperature contour plots were obtained from the software. The validation was successfully done by using the correlation between Nusselt number on impingement point and Reynolds number. The dimensionless temperature of concave plate increases when Reynolds number increases and hot air temperature decreases. The highest dimensionless temperature recorded is 0.147125 under the set of 300mm curvature radius, air temperature of 43°C, Reynolds number of 4070. The dimensionless temperature of the plate decreases with the curvature radius decreases due to the increase of heat dissipation. The dimensionless temperature increases from 0.138747 to 0.142316 when the curvature radius increases from 150mm to 300mm.

# CHAPTER 1 INTRODUCTION

Icing is one of the common causes of air accident and could cause fatalities. In flight icing and on ground icing can lead to serious trouble to the aircraft. Icing can cause stall and loss of control which is very dangerous to the passengers. Based on the statistics of NTSB, there are 52 in-flight icing events from 2010 to 2014 causing 78 fatalities (Eick, 2015).

Table 1.1: NTSB 2014 Icing Accidents (Eick, 2015)

| Date | NTSB | Location | Aircraft | Fatal | Remarks |
|---|---|---|---|---|---|
| Feb. 3, 2014 | ERA14FA112 | Bellevue, TN | Gulfstream 690C, N840V | 4 | Approach icing conditions |
| Feb. 5, 2014 | DCA14FA058 | Memphis, TN | EMB145<br>Part 121 | 0 | Wing stall, hit runway on landing, icing |
| Feb. 14, 2014 | CEN14IA139 | Gunnison, CO | Cirrus SR22, N18DN | 0 | Icing unable to maintain altitude – pull chute |
| Oct. 4, 2014 | CEN15LA021 | Dixon, IL | Raytheon 58, N345PG | 0 | LOC – uncontrolled descent, icing, substantial damage |
| Nov. 6, 2014 | CEN15FA040 | Grover Hill, OH | Cirrus SR22, N811CD | 3 | LOC - icing |
| Nov. 12, 2014 | CEN15FA044 | Clines Corner, NM | Mooney, N231JF | 1 | LOC – wx favorable icing |
| Dec. 8, 2014 | DCA15MA029 | Gaithersburg, MD | EMB-500, N100EQ | 6 | LOC – stall, icing conditions |
| Dec. 30, 2014 | CEN15LA091 | Roswell, NM | C208, N950FE<br>Part 135 | 0 | LOC in icing, landing impacted terrain short of runway |

Therefore, all the aircrafts are equipped with de-icing and anti-icing system. De-icing and anti-icing system use different energy to remove the ice including mechanical, chemical and thermal energy. Pneumatic inflatable boot (PIB), Electro Impulse De-icing (EIDI) and Electro Magnetic Expulsion De - icing (EMEDS) utilize mechanical energy while weeping wing utilizes chemical energy to remove the ice accretion. Piccolo Tube Anti Icing (PTAI) and Swirl Anti Icing (SAI) system utilizes thermal energy to prevent the formation of ice.

This project will be focus on the effect of thermal type anti-icing system on aircraft body such as nacelle lip skin and edges of wings.

## 1.1 Project Background

Aircraft icing is a serious threat to flight safety. Aircraft icing is a phenomenon that ice accretion occurs on the surfaces of aircraft. The ice is formed when supercooled water droplets in the clouds impinge on aircraft (Cao, Huang, & Yin, 2016). Icing usually occurs on some important parts of aircraft such as leading edges of wing, tails, engine inlet, windshield, and helicopter blade (Potapczuk, 2013). Ice accretion can degrade the performance of aircraft as it causes increase of weight and drag, reduction of lift and thrust. The wing surface feature changes due to the accumulation of ice. If the condition is critical, air crash may happen due to icing. For example, on 27 December 1991, Scandinavian Airlines Flight 751, a McDonnell Douglas MD-81 was forced to make an emergency landing due to icing. Clear ice was accreted on the wings of the aircraft before departure. In connection with takeoff, the clear ice loosened and was ingested by the engines. The ice damaged the engine fan stages and caused engine surges. Eventually, it led to caused engines failure. Fortunately, all 129 passengers and crew members aboard survived (Forrsberg et al., 1991). However, 51 people on USAir Flight 405 was unlucky. Ice had accumulated on the wings and eventually disrupted airflow and decreased lift. The root cause of the air crash is that the anti-ice system was switched off. The air crash had caused 27 fatalities and 21 injuries (National Transportation Safety Board, 1996).

Figure 1.1: Twin Otter aircraft with supercooled large droplets ice accretion (courtesy of NASA)

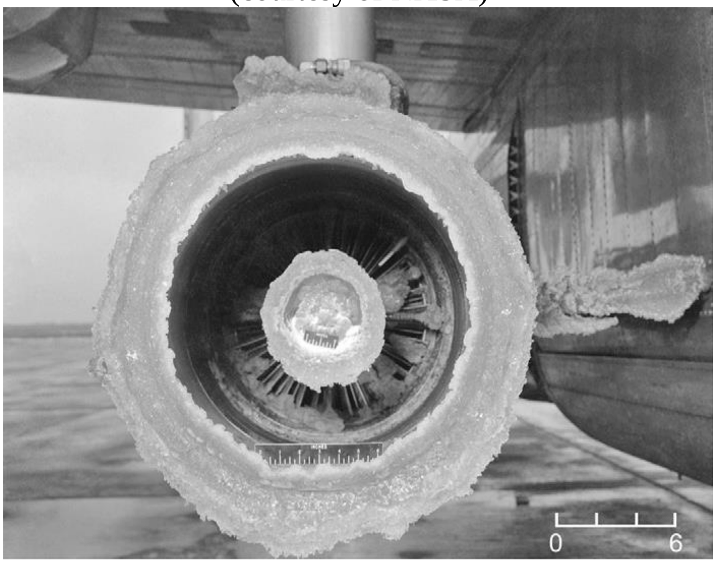


Figure 1.2: Ice formation on W24C-2 engine inlet during flight test campaign at the GRC in March 1948 (courtesy of NASA)

Therefore, ice protection system is very crucial to flight safety. There are two types of ice protection system mostly equipped in commercial aviation namely, the anti - icing system (AI) and de - icing system (DI). Anti-icing systems are preemptive system, they are activated before the flight enters icing conditions. Anti-icing systems are aimed to prevent ice forming by providing energy continuously. De-icing systems are used to periodically get rid of accreted ice when the ice has accumulated to a significant thickness (Nagappan, 2013).

Anti-icing system delivers energy or chemical flow continuously to a surface to prevent the formation of ice. One of the famous hot air anti-icing systems is Piccolo Tube Anti-Icing system (PTAI). Piccolo tube is a tube with a series of in-line or staggered holes placed inside the wing leading end near to its inner surface as shown in Figure 3. The hot air is blown out from the engine compressor, is then passed through the piccolo tube. The hot air is ejected from the piccolo tube holes at high velocity and impinge on to the inner surface of the wing leading edge. Heat is conducted from wing inner surface to outer surface so that the outer surface of the wing leading edge is hot enough to prevent ice accretion (Sreedharan, Nagpurwala, & Subbaramu, 2014).

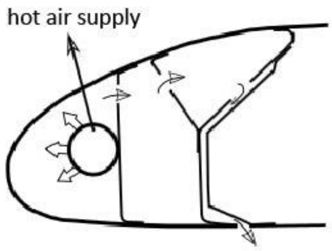


Figure 1.3: Typical thermal anti-icing system using piccolo tube

Swirl Anti-Icing (SAI) system is. Hot air from the jet engine is directed to the D-chamber at high pressure by a supply pipe. The end of the nozzle is bent 90° so that the hot air can be expelled at high velocity substantially along a tangent to the middle circle of the D-chamber. The air with high temperature and velocity exits from the nozzle and mixes with the cool stationary air in the D-chamber, which causes large amount of cold air entrained by hot air. Eventually, the mixed air swirls circularly around the annular D-chamber (Herman, 1987).

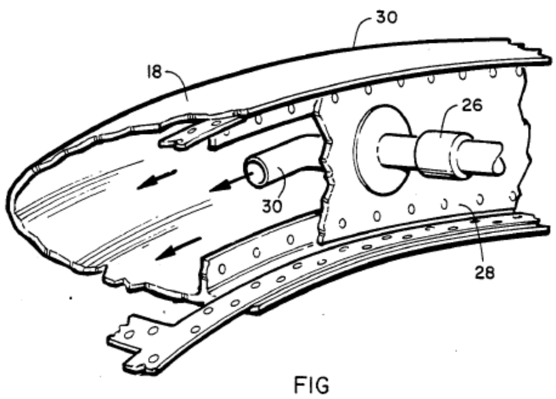


Figure 1.4: Annular inlet leading edge showing novel hot gas nozzle

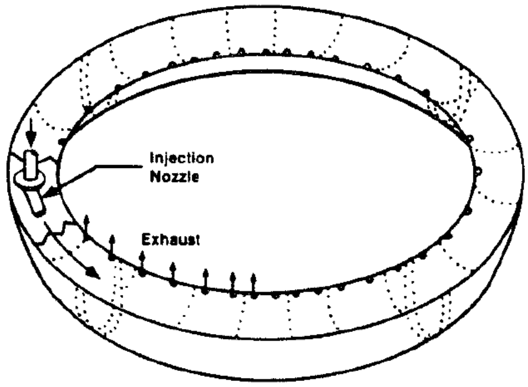


Figure 1.5: Swirl anti-icing system

## 1.2 Problem Statement

Anti-icing system is very important to aviation safety. The system is installed to prevent ice accretion on the body of aircraft. Ice accretion degrades the performance of the aircraft and may cause air crash. The impingement flow of hot air from Piccolo tube creates hotspot on nacelle lip skin and edges of wings. Improper heating may cause high thermal stress and damage the nacelle lip skin and edges of wings. Therefore, it is important to investigate the temperature profile of the hotspot on concave plate.

## 1.3 Objectives

1. To validate the simulation result with previous experimental result of literature.
2. To study the effect of Reynolds number of impingement flow and hot air temperature on temperature distribution of concave plate.
3. To investigate the effect of concave radius on the surface temperature distribution in impingement flow study.

## 1.4 Scope of Research

In this research, hot air impingement flow onto concave plate is simulated by using ANSYS Fluent 19.2. The temperature distribution is analyzed from the contour plot. The validation is done by comparing the simulation result with the reference literature from Mohanty and Tawfek (1993). Nusselt number on impingement point is compared by using the correlation created by them.

Next, the effects of increasing Reynolds number and air temperature on the temperature distribution are studied. The Reynolds number is increased by increasing the air velocity. The air velocity studied are 20m/s, 22m/s, 24m/s, 26m/s and 28m/s. Moreover, the air temperature studied are 43°C, 48°C, 53°C and 58°C.

For the third objective, the effects of increasing curvature radius on the temperature distribution is studied. The curvature radii studied are 150mm, 200mm, 250mm and 300mm. The temperature distribution is studied form the contour plot and the temperature of the impingement point

# CHAPTER 2 LITERATURE REVIEW

## 2.1 Ice Accretion

Ice accretion on aircraft can be happened on the ground and in the air. On the ground, slush, snow, clear ice or combination of them were caused by the snow or freezing rain falling on the aircraft. Likewise, icing can be formed on aircraft wings in ambient temperatures above freezing due to the presence of below-freezing fuel in the wing tanks (Thomas, Cassoni, & MacArthur, 1996). In-flight icing commonly happens during the take-off or landing phase of a flight, when the aircraft need to fly through clouds in which the temperatures are at or below freezing point (Saeed, 2003). Supercooled water droplets in clouds which are in metastable condition is the cause of icing. The droplets may hit the surface or carry away from it. When the aircraft comes across these droplets, they may either immediately change phase upon impact, or may form a thin film of water and collect into droplets due to surface tension. The droplets may be swept off from the surface by aerodynamic forces or freeze (Thomas et al., 1996).

Lynch and Khodadoust (2001) have addressed the aerodynamic performance and control degradations caused by various types of ice accretions on the lifting surfaces of fixed wing aircraft. There are four types of ice accretion were tested including initial in-flight leading-edge ice accretions, runback and “ridge” ice accretions, large in-flight ice accretions and ground frost/ice accretions. Ice accretion causes maximum lift reductions, the corresponding stall angle reductions, resulting drag penalties, and trailing-edge control surface anomalies. Runback and ridge ice accretions can cause catastrophic damage. It can be formed on leading-edge ice protection system Their test results had proved the maximum lift losses up to 80% for some single-element geometries. For larger glaze ice accretions, maximum lift losses approaching 60% can be occurred on single element lifting surfaces.

Pouryoussefi et al.(2016) have studied the effects of icing on an NACA 23012 airfoil. The aerodynamic performance of clean airfoil, runback ice, horn ice, and spanwise ridge ice were compared at a Reynolds number of $0.6x10^6$. Through their experiment, they found that the aerodynamic performance of the airfoil is worsened significantly by spanwise ridge ice. The stall angle decreases approximately 10° and the maximum lift coefficient drops about 50% which is dangerous for an aircraft. Next, horn ice causes the stall angle to decrease about 4° and the maximum lift coefficient to reduce up to 21%. Lastly, runback ice has the least effect on the flow pattern around the airfoil. The stall angle decreases 2° and the maximum lift reduces about 8%.

Swetha et al. (2019) have predicted the ice shape, thickness of ice and mass caught during the accretion. Three numerical tools or modules including FENSAP-ICE, DROP3D and ICE3D have been used to simulate the ice accretion over an airfoil. The airfoil taken for the study is NACA0012. The reference conditions are as follow,

Table 2.1: Condition of Simulation

| | |
|---|---|
| Characteristic length | 0.914 m |
| Air velocity | 100 m/s |
| Air static temperature | 262 K |
| Air static pressure | 101325 Pa |
| Reynolds number | $7.4136 x10^6$ |
| Mach number | 0.308 |
| Liquid Water Content (LWC) | 0.0007 $kg/m^3$ |
| Droplet diameter | 20 microns |
| Water density | 1000 $kg/m^3$ |

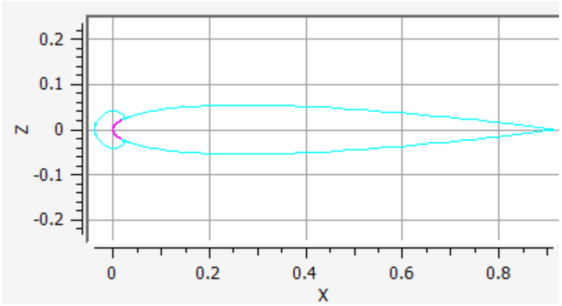


Figure 2.1: Shape of ice at time of accretion= 100min

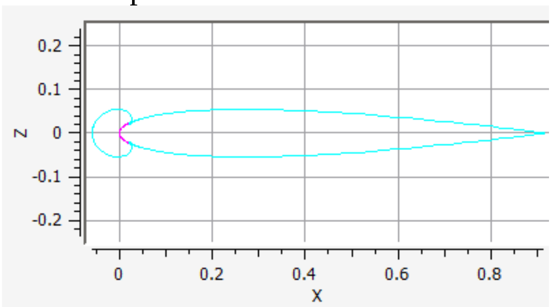


Figure 2.2: Shape of ice at time accretion= 150min

They found that the total time of accretion is directly proportional to the mass of ice accreted.

Liu et al. (2019) developed a three-dimensional aircraft ice accretion model based on the numerical solution of the unsteady Stefan problem. For this model, the temperature evolution in the ice layer is simulated directly for both the rime ice and the glaze ice. The shape of ice is compared between experimental, LEWICE model and current model. The model has well predicted the upper and lower icing limits but overestimated the thickness of the ice layer near the stagnation point.

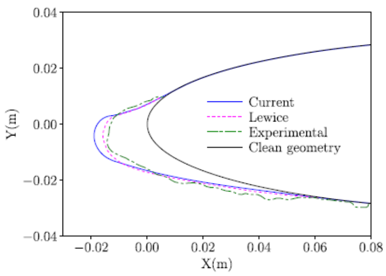


Figure 2.3: Ice shapes comparison for NACA0012 run 405

## 2.2 Anti-Icing and De-icing

Rosenthal and Nelepovitz (1985) have tested the performance of swirl anti-icing system and compared it to Piccolo tube anti-icing system. Unevaporated runback for the swirl system is about 20 percent less than that for the Piccolo system. Swirl system is simple and light in weight. Therefore, the construction of the system is more reliable, easier inspectable, and easier maintenance.

Hann et al. (2020) have identified the most energy efficient ice protection system (IPS) method among anti-icing system, conventional de-icing system and de-icing with parting strip. A parting strip (PS) is a special heating zone that is constantly heated, and can be used to minimize the energy needed for de-icing (SAE International, 2016). The parting strip is usually located near the stagnation point. It can greatly prevent ice from covering the entire leading-edge. The ice will be accumulated into an upper and a lower segment. This separation leads to greater aerodynamic forces on the ice. Hence, by eliminating the ice bridge formed at the stagnation point, ice shedding efficiency increases.

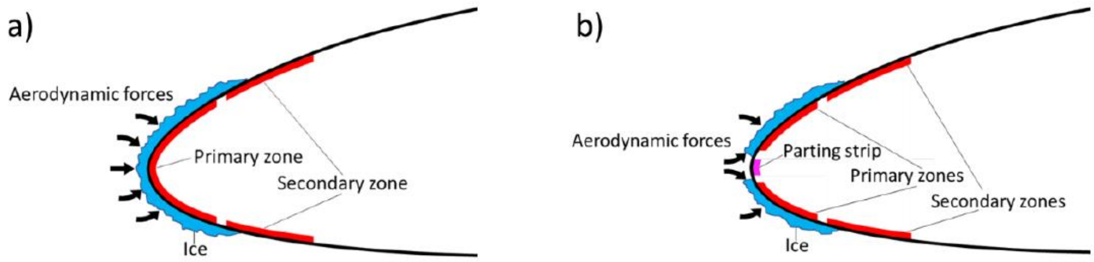


Figure 2.4: Schematic layout of the heating-zones for the conventional de-icing (a) and de-icing with parting strip (b).

The results show that anti-icing is the least energy-efficient ice protection system. De-icing has proven to be the most efficient system as it requires much lower heat loads at all temperatures. A conventional IPS, with a periodically heated leading-edge, and a parting strip IPS, with a continuously heated small area, were tested for de-icing. De-icing with the parting strip needs 50% less energy than a conventional de-icing system.

Li et al. (2020) have conducted an experimental study on a hot-air-based anti-/de-icing system for aeroengine inlet guide vanes (IGV). The experimental results reveal quantitatively that, more than 85% of the thermal energy supplied by the hot-air stream was dissipated by the convective heat transfer via the frozen-cold airflow over the surface of the IGV model for the anti-/de-icing operation, while only less than 15% of the supplied thermal flux would be dissipated by heat conduction via the substrate of the IGV model or supporting parts. The thermal energy dissipation characteristics are not affected by the operation parameters of the hot-air supply system. However, the ice accretion process over the surface of the IGV model is greatly affected by the operation parameters like temperature and mass flow rate of the hot-air stream.

The effect of hot air jet arrangement from a Piccolo tube in aircraft wing anti-icing system was studied by Khalil et al. (2020). Anti-icing structure for a usual aircraft wing of NACA 23014 airfoil profile was used and studied numerically.

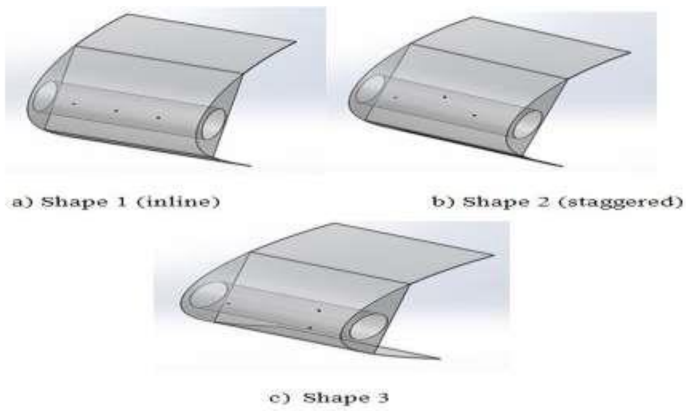


Figure 2.5: Three Different Jet Arrangement

Based on the simulation, Shape 3 is the best arrangement that covers surface on leading edge with high temperature more than other shapes.

## 2.3 Experimental Impingement Heat Transfer

Perry (1954) has investigated the heat transfer by convection from a hot gas jet to a plane surface. He found that when the jet impingement angle decreases from 90 degrees to 15 degrees, the heat transfer coefficient decreases as well. He also plotted the heat transfer contours when the jet impingement angle was 90 degrees, 30 degrees and 15 degrees. It is proven that the contours for 90 degrees are almost symmetrical in both directions, horizontally and vertically. At 30 and 15 degrees, the spread is not symmetrical as the gases are increasingly pushed forward. As the result, the heat transfer is relatively higher in the forward jet direction than side and backward direction.

Rotta (1967) has studied the rate of heat transfer in a supersonic, turbulent, boundary layer on a concave wall. When the pressure is remained constant along the wall, there is about 20% increase in the rate of heat transfer due to the streamwise curvature of the wall on concave wall. Under same condition, a decrease was detected on convex wall. The change in heat transfer rate is caused by the changes of turbulent mixing at the curvature.

Gau and Chung (1991) studied the surface curvature effects on impingement cooling flow structure and heat transfer around concave and convex side of semicylindrical surface. For convex surface, there is a series of three-dimensional counterrotating vortices close to the wall on the stagnation point. The large the radius of surface curvature the greater the size of the counterrotating vortices, which leads to the increase of Nusselt number at stagnation point. However, the heat transfer is decreased in the region away from the stagnation point because the flow can be stabilized by the centrifugal force due to the surface.

Chan et al. (2002) have investigated the effect of jet Reynolds number and dimensionless slot nozzle-to-impingement surface distance on the heat transfer distribution of convex surface. Nusselt number at stagnation point increases steadily with jet Reynolds number.  Moreover, the average circumferential Nusselt number around semi-circular convex surface reduces at a higher rate than that happens laterally along a flat surface.

Roy and Patel (2003) have investigated the correlation between average Nusselt number and the jet angle on flat surface. They have studied heat transfer of jet impingement in two different boundary conditions which are open and confined conditions. The peak Nusselt number in confined conditions was higher than open conditions. Increasing jet impingement angle can lead to increase in Nusselt number.

Lee et al. (2007) have studied surface heat transfer characteristics of a heated slot jet impinging on semi-circular surface. Nusselt number at stagnation point decreases with increasing tilt angle at the constant Reynolds number. Maximum heat transfer coefficient is further from the stagnation point when the tilt angle increases or the distance between the nozzle and collision surface decreases.

The heat transfer characteristics of the inclined impinging air jets at small nozzle-to-plate spacing less than one nozzle diameter was determined by Choo et al. (2012). They found that there is huge difference in heat transfer characteristics between small nozzle-to-plate spacings and large nozzle-to-plate spacings. Average Nusselt numbers at small nozzle-to-plate spacing increases when the inclination angle increases because of an increase in the pumping power.

## 2.4 CFD Study of Impingement Heat Transfer

Seyedein, Hasan and Mujumdar (1994) have modelled a single confined turbulent slot jet impingement using various isotropic two-equation k-ε turbulence models. The standard k-ε turbulence model is not the most suitable model to simulate the confined turbulent impinging jet. The accuracy of the results is greatly affected by the model parameters and the near-wall treatment. Low-Reynolds versions of the k-ε model are suitable for modelling of turbulent impinging jets.

Shi et al. (2002) used commercial finite volume code FLUENT 5.0 to simulate the heat transfer characteristics of a single impinging semiconfined slot jet under turbulence models, near wall treatments, turbulence intensity, jet Reynolds number and the type of thermal boundary condition on the heat transfer by using standard k-ε and RSM models. Both the models marginally overpredicted the Nusselt number distributions under some conditions. The simulated results performed well for large nozzle-to-target spacing if compared to the experimental results, but the predictions for small nozzle-to-target spacing are inadequate.

Souris et al. (2004) used $k - \varepsilon$ model and Reynolds stress model (RSM) to simulate the effect of jet Reynolds numbers of the spacing between the nozzle and the concave surface. The result shows that the highest heat transfer took place at the highest Reynolds number, and at the shortest nozzle - to-surface spacing. It is because Taylor-Görtler-type vortex is produced by the surface curvature. The vortex increases the momentum and energy transfer from air to the surface.

Chougule et al. (2011) have done a numerical study of multiple (3x3) circular air jet vertically impinging on a flat plate. It is performed with minimum cross flow arrangement. They found that the SST turbulence model gives more accurate estimation of fluid properties in impinging jet flows. The percentage results difference between the experimental and CFD analysis is ±5%. The heat transfer rate is higher for lower distance between nozzle exit and impinging plate to nozzle diameter ratio (Z/d ratio) because the impingement surface area decreases.

El-Maghlany et al. (2012) have studied the numerical simulation on the impingement of confined rectangular slot jets on flat plate. They had investigated how the number of jets on the plate at the given total mass flow rate affect heat transfer characteristics. It shows the maximum local Nusselt number is getting lower with increasing number of impinging jets from 1 to 5 jets. The results show that when the numbers of jets increase, the Nusselt number increases at constant mass flow rate.

# CHAPTER 3 METHODOLOGY

## 3.1 Modelling the Geometry

The modelling of geometry was created by using Solidworks 2020. The geometry is consisted of three parts which are nozzle, air and concave plate. The nozzle is 20mm long with diameter of 2.5mm. The length and width of the concave plate are fixed at 100mm with different radius of concave. The curvature radii of the concave plate are 150mm, 200mm, 250mm and 300mm. Air is the part between the nozzle and the concave plate. The distance between the nozzle outlet and the plate is 37.5mm which is 15 times of nozzle diameter. The geometry was drawn by using Solidworks as shown below.

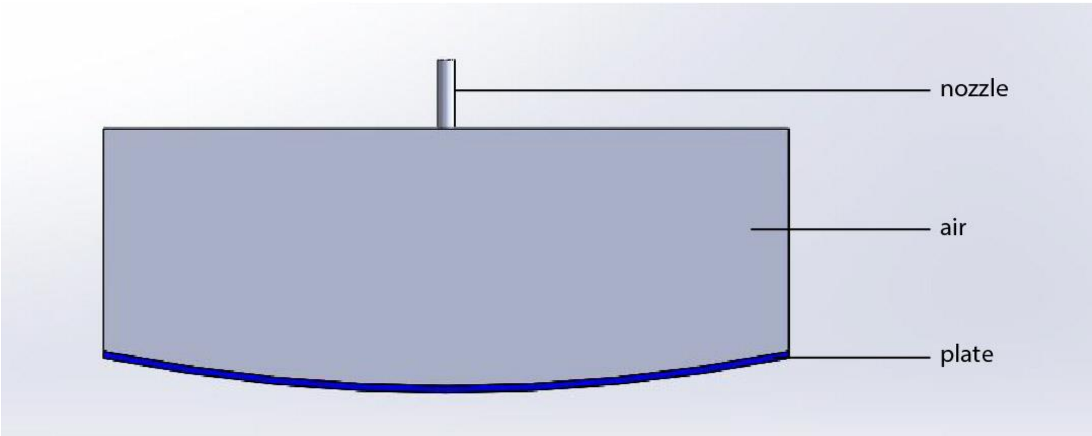


Figure 3.1: Geometry

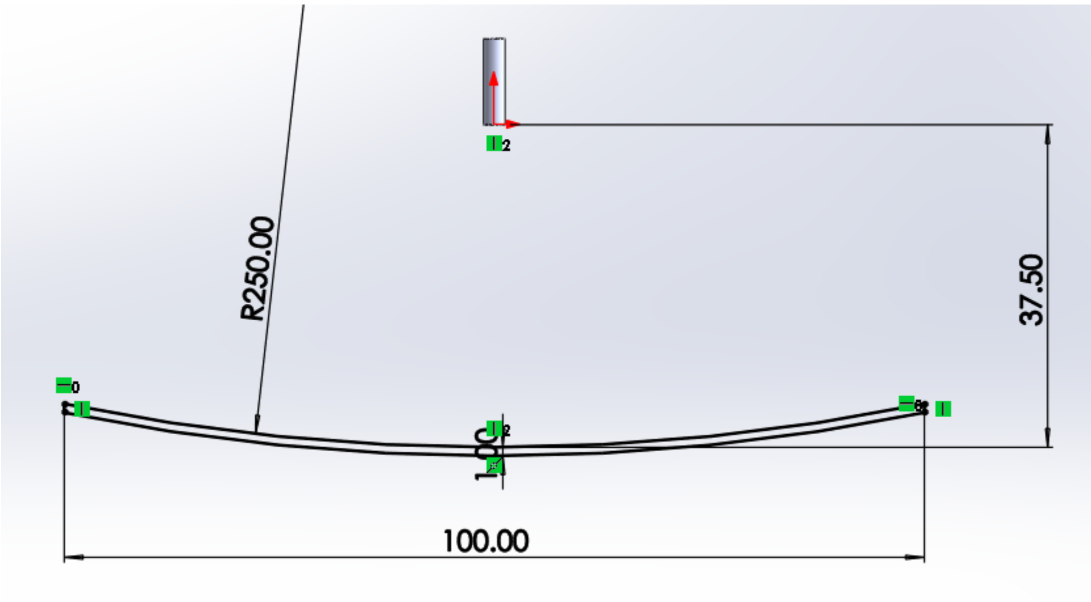


Figure 3.2: Dimension of the geometry

In order to use the geometry in ANSYS 19.2, the model was saved as STEP format. The geometry was imported into Design Modeler. The bodies were named as nozzle, air and plate. The bodies were formed as a new part.

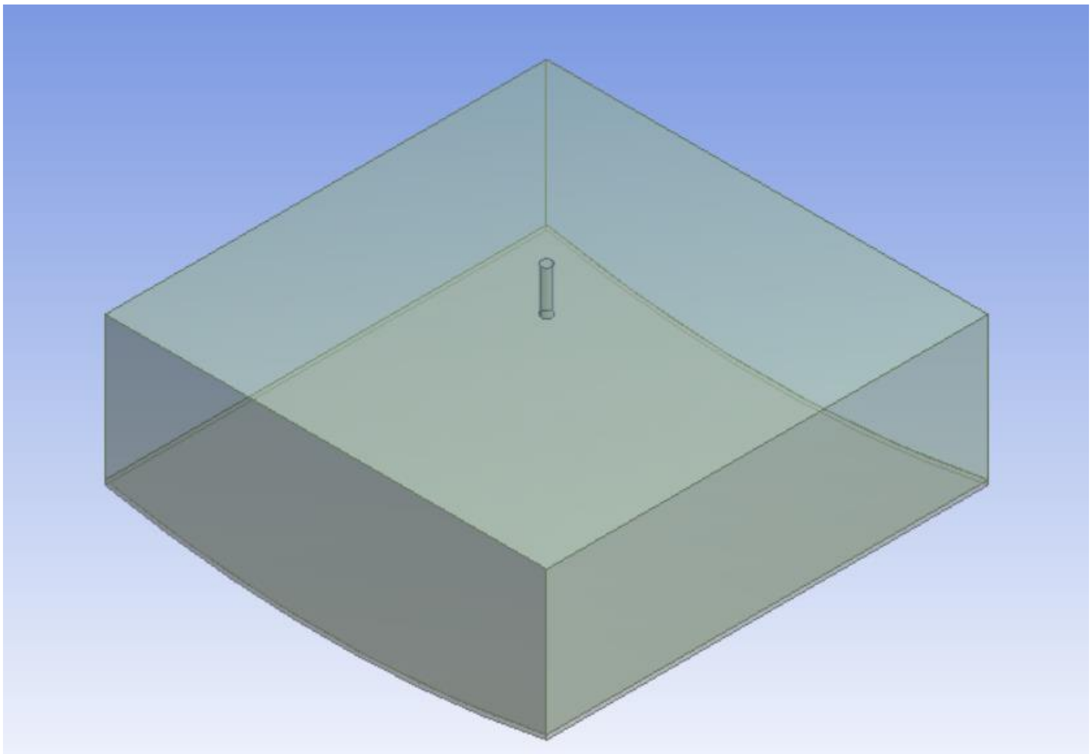

Figure 3.3: Geometry in Design Modeler

## 3.2 Mesh Creation

There are two methods were used. Multizone meshing was used for air. Sweep method was used for nozzle and plate. Element size was set at 1mm. Then, named selections were added to define nozzle wall, velocity inlet, pressure inlet and outlet. The skewness of the mesh is below 0.85. It indicates the mesh quality is good.

## 3.3 Setting Up Simulation

### 3.3.1 Models

For model part, energy equation was enabled. $k$-$\omega$ model with SST was used. Shear stress transport (SST) turbulence models consists of the advantages of the $k$-$\varepsilon$ and $k$-$\omega$ models, with a blending function that activates the $k$-$\varepsilon$ model in the core region of the flow and shifts to the $k$-$\omega$ model for the near-wall region treatment. Referring to Olsson (2004) and Akansu (2006), the SST is better in predicting the near-wall turbulence compared to other eddy viscosity models. This is crucial for a precise prediction of the turbulent wall heat transfer. Viscous heating was enabled.

### 3.3.2 Material

Nozzle and air were defined as air in Ansys. Plate was defined as aluminium. The properties of air and aluminium were set as follows.

Table 3.1: Properties of Air

| Properties | Value |
|---|---|
| Density | Ideal gas |
| Specific Heat | 1006.43 J/kg·K |
| Thermal Conductivity | 0.0242W/m·K |
| Viscosity | Sutherland |
| Molecular Weight | 28.966 kg/kmol |

Table 3.2: Properties of Aluminium

| Properties | Value |
|---|---|
| Density | 2719 $kg/m^3$ |
| Specific Heat | 871 J/kg·K |
| Thermal Conductivity | 202.4 W/m·K |

### 3.3.3 Boundary Conditions

The temperature of pressure inlet and outlet were set at 27° C. The velocity of inlet air was set at 20, 22, 24, 26 and 28m/s. The temperature of the inlet air was set at 43, 48, 53 and 58° C. The turbulence specification method of velocity inlet was intensity, 5% and hydraulic diameter, 0.0025m.

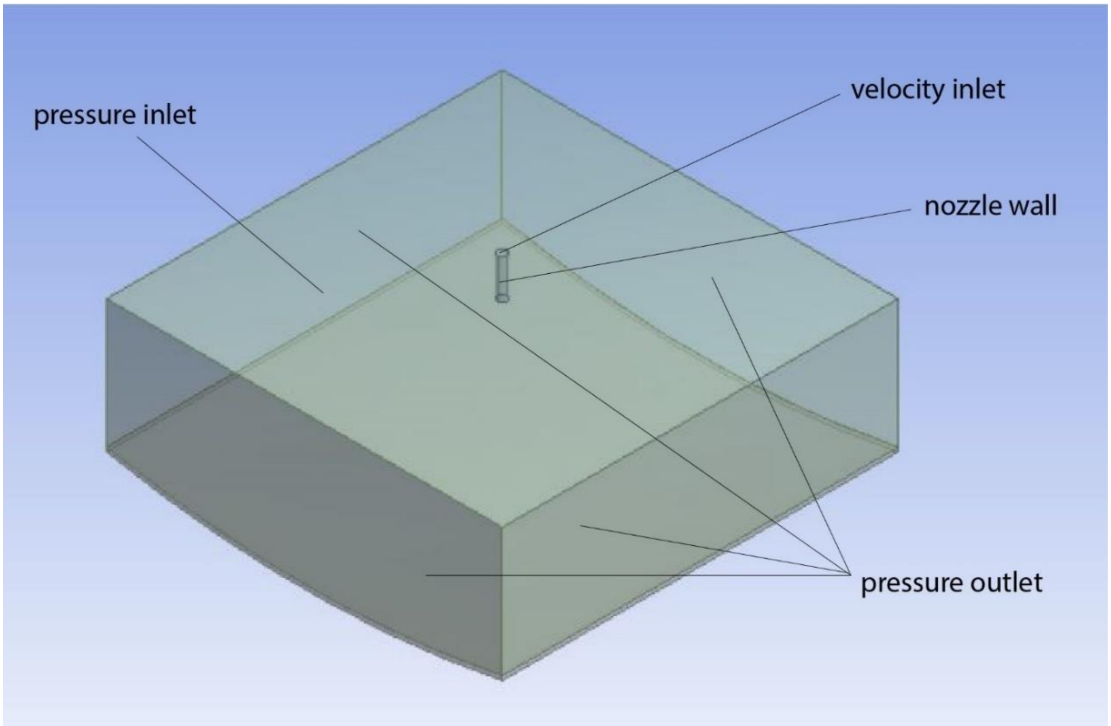


Figure 3.4: Boundaries of the Geometry

### 3.3.4 Solution

SIMPLE scheme was applied for pressure-velocity coupling. The spatial discretization settings are shown as table below.

Table 3.3: Spatial Discretization Settings

| | |
|---|---|
| Gradient | Least Squares Cell Based |
| Pressure | Standard |
| Density | Second Order Upwind |
| Momentum | Second Order Upwind |
| Turbulent Kinetic Energy | First Order Upwind |
| Specific Dissipation Rate | First Order Upwind |
| Energy | Second Order Upwind |

The solution control was maintained. The solution limits were changed on maximum absolute pressure, maximum static temperature and maximum turbulent viscosity ratio. The limits were set at 1e+20.

Standard initialization was used. The conditions were computed from velocity inlet. The X, Y and Z velocity were set at 0 while the temperature was set at 27° C. The calculation was started and ended when it converged. It took around 250 to 300 iterations to reach convergence.

## 3.4 Validation of Results

### 3.4.1 Result Comparison with Literature

Nusselt number on impingement point was compared with the correlation made by Mohanty and Tawfek (1993) The correlation is stated as follow.

For H/D from 10 to 16.7, Re from 4,860 to 15,300:

$$Nu_0 = 0.15Re^{0.701}\left(\frac{H}{D}\right)^{-0.25} \tag{1}$$

The setup and boundary conditions were set similar with the literature. Simulation was run and the result was compared to Nusselt number calculated using formula (1). Percentage error was calculated.

The velocity of the air is calculated by using the formula as below.

$$v = \frac{Re \cdot \mu}{\rho_{air} D} \tag{2}$$

The local heat transfer coefficient, $h$ is calculated by using the formula as below.

$$h = \frac{\emptyset_q}{T_0 - T_{air}} \tag{3}$$

By obtaining the maximum heat flux from software, Nusselt number on the impingement point is calculated by using the formula as below.

$$Nu_0 = \frac{hD}{\lambda_{air}} \tag{4}$$

### 3.4.2 Mesh Independence Test

Mesh independence test was carried out to determine the optimum number of meshes to attain the results that are independent to the mesh structure. 3 different element sizes including 0.9mm (676931 cells), 1.0mm (511229 cells) and 1.1mm (417825 cells) were run under same condition. The maximum temperature obtained by three different element sizes are compared. The suitable element size was selected by optimizing the acceptable accuracy and the computational time. 300mm curvature radius, 28m/s air velocity with different hot air temperature were tested. The maximum temperature of the plate was collected for 3 different element sizes. From the results, the difference in temperature is small when the element size increases. The computational time for 1.1mm is around 15 minutes, for 1.0mm is around 30 minutes and for 0.9mm is around 45 minutes. Therefore, element size of 1.0mm is chosen based its acceptable computation time.

Table 3.4: Mesh Independence Test Results

| Temperature of hot air | 0.9mm (676931 cells) | 1.0mm (511229 cells) | 1.1mm (417825 cells) |
|---|---|---|---|
| | Maximum Temperature of Plate (°C) | | |
| 43 | 29.38589 | 29.35400 | 29.32903 |
| 48 | 30.09127 | 30.04986 | 30.01742 |
| 53 | 30.78655 | 30.73568 | 30.69586 |
| 58 | 31.47225 | 31.41180 | 31.36471 |

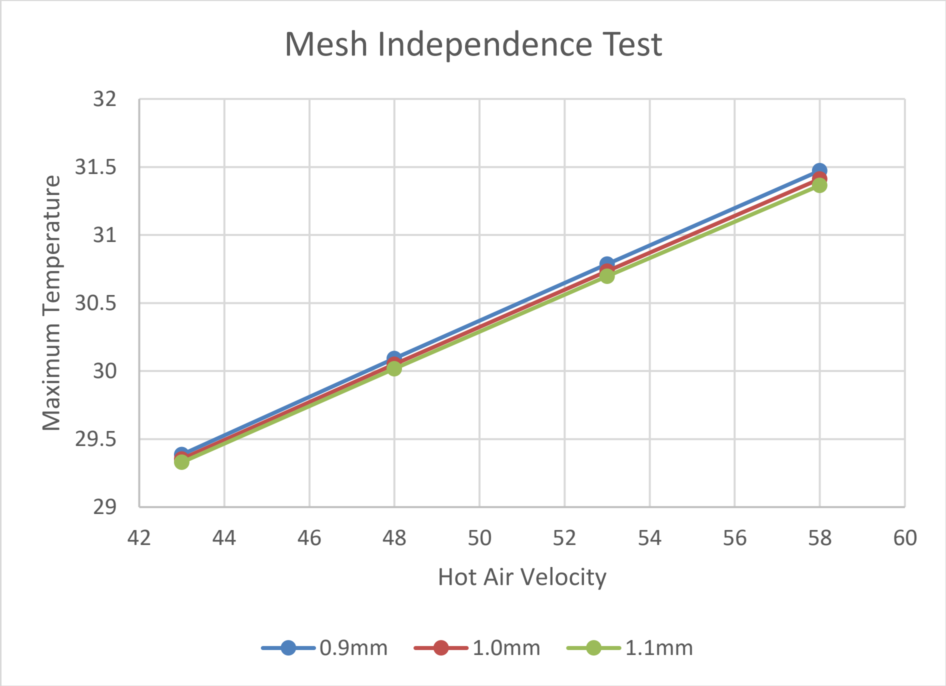


Figure 3.5: Graph of Mesh Independence Test